Spread Spectrum CDMA Systems for Subband Image Transmission

Po-Rong Chang, *Member, IEEE*

***Abstract*— This paper investigates the application of spread spectrum code-division multiple access (SS-CDMA) techniques to subband image transmission over a bandlimited radio channel. For the transmission of images over SS-CDMA AWGN channels, a subband coding scheme that divides the image information into a number of independent data streams using an analysis filter bank, each of which is multiplied by its unique signature PN code, enables the transmission of these data streams via multiple parallel virtual channels created by their corresponding PN codes. With a sufficiently large number of streams, the total signal is able to fit within the narrow radio channel bandwidth even though the total bandwidth of all the signals may exceed the channel bandwidth. At receiver, each received signal is separately recovered at the decoder by multiplying its PN code and integrating over the code length in order to obtain the desired subband. All the recovered subbands are then reassembled by a synthesis filter bank into a close reproduction to the original image. Additionally, for color subband image transmission, color images are first transferred to luminance (Y) and two chrominance components (I, Q). Each component is then decomposed independently into several subbands for SS-CDMA transmission. Therefore, a number of additional PN codes are required to support the transmission of the chrominance signals over the CDMA channels whereas the luminance signal was treated in the same manner as monochrome pictures. Moreover, SS-CDMA allows more than one image to be transmitted and be accessed simultaneously at the same limited channel bandwidth. If all the product signals for different images are transmitted over the SS-CDMA AWGN channel with perfect power control, the performance is the same as if the data were transmitted in a single stream. However, the quality of the farther received images would be degraded when the near-far problem occurs. In this paper, the image quality of both the monochrome and color subband image transmission via SS-CDMA AWGN channels is evaluated for both perfect and imperfect power control cases.**

I. Introduction

IMAGE transmission is one of the future potential data services over mobile data networks or PCS systems. Due to limited radio spectrum, however, only a finite number of radio communication channels can be shared by mobile users. As a result, image data should be compressed before transmission in order to efficiently use each radio channel. CCITT recommends the international standard H.261 [1] for video transmission at $p \times 64$ kb/s $(p = 1, 2, \cdots, 30)$, where the intended applications are videophone and videoconference. The video formats adopted are CIF (Common Intermediate Format) and QCIF with a maximum image rate of 29.97 frames/s, which implies uncompressed bit rates of 36.45 and 9.115 Mb/s, respectively. Recently, transmission of compressed video signal coded by H.261 over a digital cordless telephone system has been experimented by N. MacDonald [2]. He reported that ARQ (Automatic Repeat Request) by error-detection is the best error-recovery method to optimize the video picture quality transmitted through a digital cordless telephone system. However, the main problem in his system is that the picture quality is governed by the throughput variation caused by the retransmission in ARQ and the low bit-rate capacity of the radio link.

In order to achieve the maximum image quality and spectrum efficiency, code division multiple access (CDMA) techniques [3]–[5] are applied to the image transmission system, where a splitting process is required to divide the image information into a large number of independent data streams, each of which is transmitted using one of the signature codes in the CDMA system, and is then spread to full channel bandwidth. In other words, higher data rates are achieved by allocating more than one code to a single image. Moreover, CDMA allows more than one image to be transmitted and be accessed simultaneously and dynamically with no waiting time at the same limited channel bandwidth. This scheme is termed as a multiple code CDMA transmission per user (image). Wyrwas *et al*. [26] proposed an alternative approach using multilevel, rather than binary, to increase the transmission bit rate. Meanwhile, in this paper, we are only interested in the multi-code CDMA systems. Gagliardi *et al*. [4] and Kitayama [5] proposed the all-optical implementations of the CDMA systems which are applied to the image transmission over a fiber optic network. Gagliardi *et al*. [4] used the laser pulsing in the form of CDMA to multiplex a set of digital video signals over a fiber network, in which data of a video source are coded into addressed lightwave pulse sequences that can be recognized and separated at the receivers. However, Gagliardi *et al*. [4] did not increase the bit rate of a single image transmission since each image has be assigned to only a single code. Kitayama [5] introduced two-dimensional (2-D) optical orthogonal signature patterns (OOSP's) to encode and decode each pixel of a binary image. His concept is based on the spatial frequency spread spectrum for image transmission over an optical CDMA network. In contrast to Gagliardi *et al*.'s method, each image is allocated more than one code using the OOSP encoding process. This would lead to a higher bit rate in the image transmission. Recently, Wang and Chang [29] applied the multi-code CDMA system with

Manuscript received November 15, 1994; revised June 10, 1995 and October 31, 1995. This work was supported in part by the National Science Council, Taiwan, R.O.C., under Contract NSC-84-2212-E-009-016.

The author is with the Department of Communication Engineering, National Chiao-Tung University, Hsinchu 300, Taiwan, R.O.C.

Publisher Item Identifier S 0018-9545(97)00648-8.

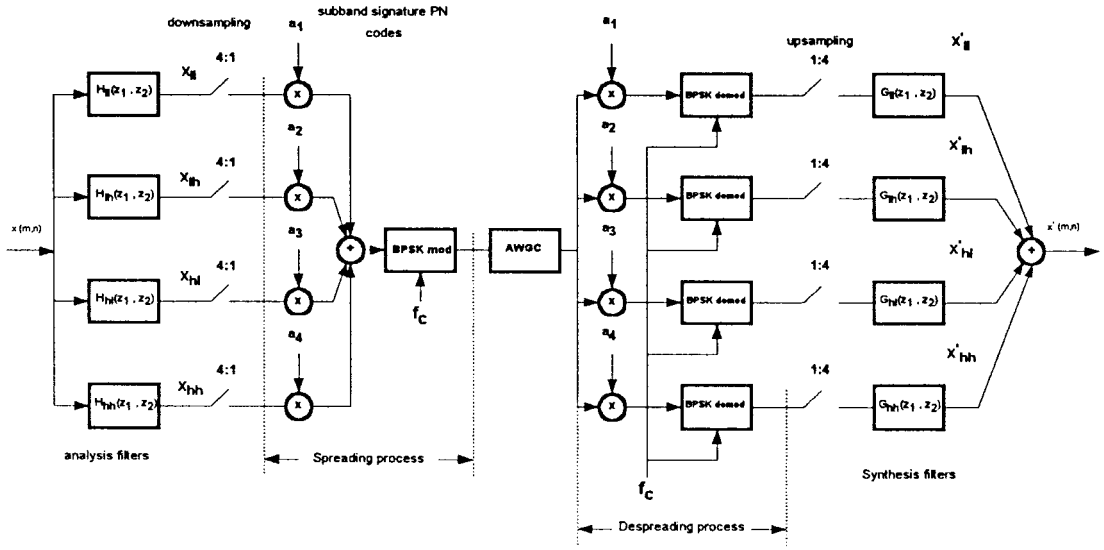

Fig. 1. Transmission of subband-coded monochrome images via SS-CDMA AWGN channels where a_i's denote the signature PN codes, f_c denotes the carrier frequency, and $M = 4$.

DPSK modulation and diversity to image transmission over indoor radio multipath fading channels. They have shown that their system is able to achieve the satisfactory received image quality via the bandlimited indoor radio channels. Another CDMA method to increase the transmission bit rate is a hybrid FDMA/CDMA scheme called the multi-carrier CDMA system. Chang and Chang [28] have shown that this hybrid FDMA/CDMA scheme is capable of achieving the high transmission bit-rate services of more than one image over a fiber optic channel.

In this paper, we propose an alternative approach to the image transmission via CDMA channels. The splitting process adopted here is based on subband coding [6]–[9] which is one of the less complex encoding algorithms. The principle of subband coding is based on the decomposition of the input image into a number of narrow bands using analysis filter bank where each band is then decimated, coded and assigned to its unique signature code separately. In addition to achieving the highest possible image quality within the narrow radio channel bandwidth and maximum spectrum utilization, the input image should be decomposed into a sufficient number of subbands where each band is spread to full channel bandwidth. After transmission, each signal sample is then independently recovered at the receiver by multiplying its code. These recovered subbands are reassembled by the synthesis filter bank into a close approximation to the input image. For dividing the image into subbands, the symmetric short kernel filters [7]–[9] (SSKF's) are used for filtering. These filters require a very small number of coefficients and are necessary to keep the implementation complexity at a low level. In Section IV, we will discuss the transmission error effects in the subband image via CDMA channels. Bit errors in an individual subband will generate error contributions at the receiver output within that frequency band. Since the channel error contributions in different subbands are expected to be uncorrelated, the total channel error variance in the recovered image equals the sum of these errors. Moreover, we will show that the total channel error variance is in proportion to the bit error rate when the bit error rate is sufficiently small. This would lead to the image signal-to-noise ratio (SNR) being inversely related to a logarithmic function of the bit error rate. However, for color image transmission, a color distortion measure in the YIQ domain is conducted to evaluate the color image quality of the reconstructed pictures via CDMA channels. This distortion measure is proportional to the bit error rate when the bit error rate is sufficiently small. Section V shows computer simulations used to evaluate the image SNR performance and the YIQ color distortion measure of monochrome and color subband image transmission by CDMA systems with 1) perfect power control and 2) without power control, respectively.

II. Transmission of Monochrome and Color Subband Images Over SS-CDMA Channels

As shown in Fig. 1, each field in a video sequence is decomposed into several components (four in the Fig. 1) using a bank of filters [i.e., $H_{ll}(z_1, z_2)$, $H_{lh}(z_1, z_2)$, $H_{hl}(z_1, z_2)$, and $H_{hh}(z_1, z_2)$] called the analysis filter bank. The lowest frequency component is a lower resolution version of the original scene, and the high-frequency components mostly carry information about the contours, edges and other finer details. These filtered signals are then downsampled to yield the subband signals. The downsampling following the analysis filter bank reduces the sampling rate of each of the M subband signals to $1/M$ times the input signal sampling rate. As result, these filters decompose the signal into M equally spaced subbands at the same time. For example, if the Quarter Common Intermediate Format (QCIF) CCITT standard videophone image of 180 pels by 144 lines is at 29.97 frames/s, it yields about 64 kb/s [1]. For $M = 4$, the bit rate of each subband can be reduced to 16 kb/s. For the transmission of these subbands at the same time in the same channel, the spread-spectrum code-division multiple access (SS-CDMA) multiplexing scheme is particularly well suited to subband

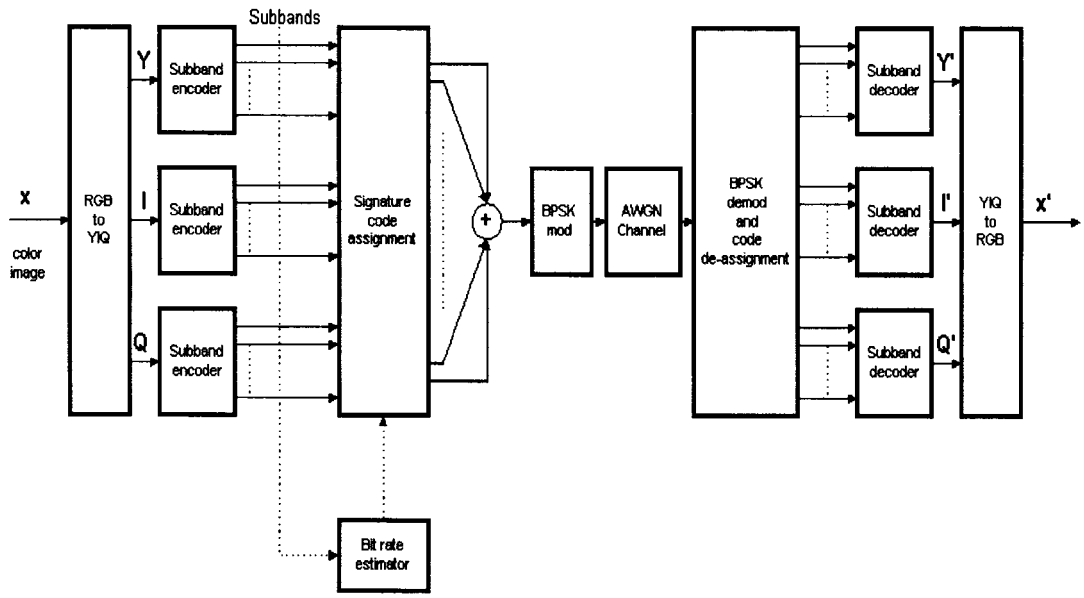

Fig. 2. General architecture of color subband image transmission via SS-CDMA AWGN channels with an adaptive signature code assignment strategy.

coding that divides the image information into multiple parallel data streams, each of which has assigned to it a signature code or an addressed PN (pseudo-random) code in the SS-CDMA system. With a sufficient number of decomposed subbands or streams, a large spreading factor can be used and yet the total signal can fit within the narrow wireless channel bandwidth. In other words, an image of rate Mr_b is disassembled (demultiplexed) into, M subsequences each of rate r_b. Each subsequence is transmitted using one of M spreading codes. Thus, the M subsequences can be transmitted at the same time in the same channel, without crosstalk. Each subsequence is independently recovered at the receiver by multiplying by its unique signature code and integrating over the sequence length. At the receiver, the M received subsequences are then decoded, upsampled, and reassembled (multiplexed) by the synthesis filter bank into a close approximation to the input scene.

The main extension from monochrome image transmission to color is the addition of two chrominance components in the above-mentioned SS-CDMA systems. In general, color pictures contain the three primary colors, red, green, and blue (RGB). However, as shown in [7], the encoding of a color image in the RGB domain is not efficient and it is better to use a color domain such as the NTSC television standard YIQ. The reason for this can be deduced from the differences between these color domains: the crosscorrelation between RGB components is high and the component variances are of the same order, while transformation of the RGB signals to the YIQ domain produces nearly decorrelated components and most of the signal energy is contained within the luminance (Y) signal. The RGB/YIQ transform is a linear transformation given by

$$\begin{bmatrix} Y \\ I \\ Q \end{bmatrix} = \begin{bmatrix} 0.299 & 0.587 & 0.114 \\ 0.597 & -0.277 & -0.321 \\ 0.213 & -0.523 & 0.309 \end{bmatrix} \begin{bmatrix} R \\ G \\ B \end{bmatrix}. \quad (1)$$

Experience has shown that the energy compactibility of RGB/YIQ transform is almost as good as the optimum Karhunen–Loeve transform [7]. Fig. 2 shows the general architecture of the SS-CDMA system for color image transmission. For encoding color images, the RGB components of color images are first transformed to YIQ components by the transformation of (1). These YIQ components are then decomposed into M_Y, M_I, and M_Q bands by their corresponding banks of analysis filters, respectively. In order to further improve the performance of the system, if the subbands have the different bit rates, more than one PN code are assigned the higher bit-rate band when its bit rate is higher than the peak channel capacity. However, more than one lower bit-rate subband may be combined to share the same PN code in order to fully utilize the channel capacity. This adaptive "merge and split" strategy is performed by monitoring the bit-rate of each subband and assigning a proper number of PN codes to a specific band according to its corresponding bit rate. For the issue of implementation and to avoid the self-interference that a high bit-rate band employing multiple codes may incur, we can use C. L. I's subcode concatenation scheme [27] to generate additional codes for that band. If a_1 is the primary code of a subband and the subband requires a higher bit rate, the additional codes, c_i, will be derived from a_1 by $c_i = a_1 \times d_i$, where $d_i \perp d_j$ for $i \neq j$. Obviously, $c_i \perp c_j$ for $i \neq j$. This orthogonality eliminates self-interference. Meanwhile, for simplified analysis, only PN codes are considered in our system.

In this paper, the focus is on intra-field subband coding and the exploitation of temporal correlation that can be carried out by a three-dimensional (3-D) subband system [10] which consists of temporal, horizontal, and vertical filterings. Undoubtedly, the SS-CDMA system can be applied to the 3-D subband system directly. However, the use of intra-field coding is motivated by the goal to keep the decoder cost low. The implementation is relatively simple since frame stores

and motion detection/estimation hardware is not required. Each field in the video sequence is represented by using 2-D subband coding [6].

A. Perfect Reconstructive Subband Coding with DPCM/PCM Coding

Recently, subband coding of images has received considerable attention and has become an effective tool for image compression. Subband coding is one of the less complex encoding algorithms which has been extensively applied to encode the HDTV signals and has produced very satisfactory results [9], [24]. For perfect reconstruction of the original picture at a very low-average entropy, Irie and Kishimoto [9] showed that there are two indices used to evaluate the performance of such a reconstruction and defined as

$$\text{PSNR} = 10\log_{10}\left[\frac{x_{pp}^2}{\sum_{i=1}^{L_p} e_i^2/L_p}\right] \tag{2}$$

and

$$\text{Entropy} = \sum_{i=1}^{L_q}[-p_i \times \log(p_i)], \quad p_i = \frac{n_i}{L_p} \tag{3}$$

where x_{pp} is the peak gray value of input image, e_i is the difference between input and output signals for the ith pixel, p_i is the probability of the quantization level i, n_i is the number of pixels which are quantized to level i, L_p, and L_q are the number of pixels and the number of the quantization levels, respectively. The entropy of (3) corresponds to the required bit rate. If the value of PSNR of (2) is extremely high, this leads to the perfect reconstruction of pictures. However, such a reconstruction may have high-average entropy which yields the long transmission delay over a bandlimited radio channel. Therefore, Irie and Kishimoto [9] introduced an integer/noninteger transformation to the design of a short-kernel filter pair (SSKF) for perfect reconstruction of subband signals at a very low bit rate (entropy). In this paper, we will apply Irie and Kishimoto's design to our CDMA image transmission system. Moreover, Vetterli [11] showed that the 2-D exact reconstruction filters for subband image coding can be developed in terms of 1-D exact reconstruction filters by using the most computationally efficient separable filter technique. The separable subband decomposition is performed in two stages using one-dimensional (1-D) filters that process the data along the rows and columns of the image data array. The input signal x is first applied to horizontal filters $H_l(z_1)$ (lowpass) and $H_h(z_1)$ (highpass), and horizontally downsampled to get the signals x_l and x_h, respectively. In the second stage of the decomposition, each of the signals x_l and x_h is applied to the two vertical filters $H_l(z_2)$ (lowpass) and $H_h(z_2)$ (highpass), and vertically downsampled to get the subband signals x_{ll}, x_{lh}, x_{hl}, and x_{hh}. For the purpose of reconstruction, the signals are merged by upsampling and filtering using the synthesis filters. The vertical synthesis filters are denoted by $G_l(z_2)$ (lowpass) and $G_h(z_2)$ (highpass), and the horizontal synthesis filters are denoted by $G_l(z_1)$ (lowpass) and $G_h(z_1)$ (highpass). In designing 1-D exact reconstruction filters, we should focus on an analysis into a two-channel system. The analysis filter bank splits the input signal into two-channel signals by processing it with a lowpass filter $H_l(z)$ in one path and with a highpass filter $H_h(z)$ in the other. The filtered signals u_0 and u_1 are downsampled by a factor of two to obtain the subband signals x_l and x_h. In a back-to-back connection, these signals are upsampled and processed by the synthesis filters with transfer functions $G_l(z)$ and $G_h(z)$. In other words, every second sample has been discarded by the downsampling and has been reinserted as a zero-valued sample by the upsampling. The aliasing distortion in the reconstruction can be removed if the synthesis filters are defined as

$$\begin{cases} G_l(z) = H_h(-z) \\ G_h(z) = -H_l(-z) \end{cases}. \tag{4}$$

Therefore, the Z-transform of the reconstructed signal output $y(t)$ can be found as

$$Y(z) = \frac{[P(z) - P(-z)]X(z)}{2} \tag{5}$$

where

$$P(z) = H_l(z)H_h(-z). \tag{6}$$

It is desirable to choose the filters $H_l(z)$ and $H_h(z)$ so that $Y(z)$ is a perfect reconstruction, but possibly delayed, replica of the input signal $X(z)$, in the absence of coding and transmission error. Quadrature mirror filters [12] (QMF's) have been proposed and widely used as analysis and synthesis filters in subband coding of images. However, [9] showed that QMF's do not permit reconstruction to be exact, although the reconstruction error can be made very small by using long tap filters. As shown in [9], QMF filter pairs of 12-tap and less do not provide satisfactory perfect reconstruction results since the difference between the entropy of an input image and the average entropy of subband signals is very small. For video and digital image applications, use of such long tap filters, while not providing any significant coding gain, may increase the hardware complexity.

Since the processing of video signals in wireless channels involves high sampling rates, it is very desirable to keep the filter bank complexity low. Symmetric short-kernel filters (SSKF's) have been considered as the low-complexity subband decomposition and reconstruction filter pairs because of the simplicity in implementation [8]. Furthermore, it has been demonstrated in [9] that SSKF pairs can effectively reduce the average entropy of subband signals by an integer/noninteger transformation. The SSKF's are the symmetric short filters which are obtained by factoring $P(z)$ into linear phase components. D. Le Gall *et al.* [8] showed that an example of a product filter with the simplest coefficients is

$$P(z) = (\tfrac{1}{2} + \tfrac{1}{2}z^{-1})(\tfrac{1}{2} + \tfrac{1}{2}z^{-1}). \tag{7}$$

From (6), the lowpass and highpass analysis filters are

$$\begin{cases} H_l(z) = (\tfrac{1}{2} + \tfrac{1}{2}z^{-1}) \\ H_h(z) = (\tfrac{1}{2} - \tfrac{1}{2}z^{-1}) \end{cases}. \tag{8}$$

In the 2-tap analysis filters of (8), low-band signal $x_l(t)$ and high-band signal $x_h(t)$ are determined by a pair of successive input signals $x(t)$ and $x(t-1)$ by the following equations:

$$x_l(t) = \frac{[x(t)+x(t-1)]}{2} \tag{9}$$

$$x_h(t) = \frac{[x(t)-x(t-1)]}{2}. \tag{10}$$

Similarly, from (4) and (8), the synthesis filters are

$$\begin{cases} G_l(z) = H_h(-z) = (\frac{1}{2} + \frac{1}{2}z^{-1}) \\ G_h(z) = -H_l(-z) = -(\frac{1}{2} - \frac{1}{2}z^{-1}) \end{cases}. \tag{11}$$

The 2-tap filters of (8)–(11) can be realized using a small number of shift and add operations. The use of general multipliers is avoided. This leads to a simple and computationally efficient subband coding implementation. Note that the decomposition of the input image can be extended to more than four bands by repeating the separability process to each subband image in a tree-structured manner.

Observing the expression of (9) and (10), the number of output signal levels is twice that of input signal levels when one of the successive input signals $x(t)$ and $x(t-1)$ is an even number and the other is an odd number. In this case, the filtered-output signals $x_l(t)$ and $x_h(t)$ are found to be noninteger which means the number always has a value of 0.5 attached to it. For the perfect reconstruction purpose, all signal values have to be preserved losslessly even when the number of output levels is increased. Irie and Kishimoto [9] have shown that the average entropy of subband signals can be reduced if the number of subband signal levels is reduced to less than or equal to that of input signals. An integer/noninteger transform was proposed to reduce the number of subband signal levels in order to achieve the perfect reconstruction at a very low entropy. When the high-band signal $x_h(t)$ is found to be a noninteger number, a transformation of the low-band signal from a noninteger number to an integer number by subtracting 0.5 from the original signal is proposed to obtain a new low-band signal $x_l^n(t)$. Thus, the new low-band signal $x_l^n(t)$ is used instead of the conventional signal $x_l(t)$ and is shown as follows:

$$x_l^n(t) = \begin{cases} 0.5 \times [x(t)+x(t-1)] - 0.5 & \text{if } x_h(t) \text{ is a noninteger} \\ 0.5 \times [x(t)+x(t-1)] & \text{if } x_h(t) \text{ is an integer} \end{cases}. \tag{12}$$

From (12), as a result, the number of low-band signal levels can be reduced to half of the original one. At the receiver, the original low-band signal $x_l(t)$ can be retrieved by adding 0.5 to the decoded low-band signal according to the following equation:

$$x_l(t) = \begin{cases} x_l^n(t) + 0.5 & \text{if } x_h(t) \text{ is a noninteger} \\ x_l^n(t) & \text{if } x_h(t) \text{ is an integer} \end{cases}. \tag{13}$$

The proposed 2-tap filters can greatly reduce the entropy of the subband signals much better than obtained by conventional 2-tap SSKF filter, while maintaining distortion-free encoding when the subband signals are quantized at 10 b for perfect reconstruction.

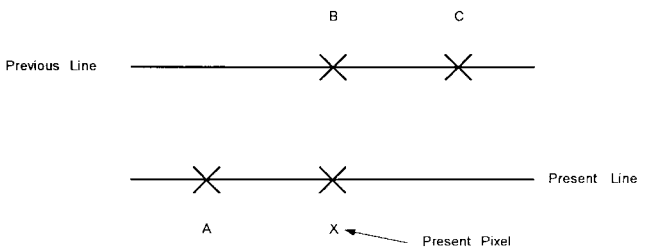

Fig. 3. Configuration of pixels used for prediction.

The entropy can be further reduced by a differential pulse code modulation (DPCM) in the based band. The pixel configuration for the 2-D prediction is shown in Fig. 3. The predicted value is given by

$$\hat{x}_A = bx_B + cx_C + dx_D \tag{14}$$

where x_B, x_C, and x_D are previously reconstructed pixels, and $\hat{x}_A$ is the prediction of the present pixel. The weighting factors, b, c, and d are chosen to be 0.5, 0.25, and 0.25, respectively. The prediction error signal is then quantized by a symmetric nonuniform quantizer. Variable-length code (Huffman) is used to encode the quantized prediction error signal of the baseband. For the higher frequency bands, only a relatively small number of samples carry significant information and the visual quality of the reconstructed image depends on their representation. Gharari and Tabatabai [7] proposed a highly efficient nonuniform symmetric quantizer with center dead zone to quantize the high bands. The dead zone is used to eliminate the picture noise. The input values in the active region are then uniformly quantized to L levels. Usually, Huffman codes are used to encode the quantized nonzero pixel values. Meanwhile, the quantized high bands are observed to have a large number of connected areas of zeros. Therefore, run-length coding techniques are implemented as one-dimensional codes for this purpose.

B. Channel Error Protection Strategies

Among various forward error correction (FEC) schemes, the Reed–Muller (RM) code is one of the useful codes for correcting random errors in the SS-CDMA channels. The RM code is a specific subclass of Euclidean geometry (EG) codes [15]. A $(\mu, 1)$th-order EG code is called a μth-order RM code. The μth-order RM code of length $n = 2^m - 1$ has the following parameters:

$$\begin{aligned} k &= \sum_{i=0}^{\mu} \binom{m}{i} \\ d_{\min} &= 2^{m-\mu} - 1 \\ J &= 2^{m-\mu} - 2. \end{aligned} \tag{15}$$

Lin and Costello [15] showed that the μth-order RM code is capable of correcting

$$t_{ML} = 2^{m-\mu-1} - 1 \tag{16}$$

or fewer errors. Note that, at each step of orthogonalization, only J orthogonal error sums are used to determine an error sum for the next step. The RM code spreads each channel bit with $mN_c/2^m$ chips as compared to N_c for an uncoded system, where N_c is the number of the spreading sequence in SS-CDMA systems. In addition, since $J = d_{\min} - 1$, RM codes are completely orthogonalizable and are generated recursively as follows:

$$H_0 = 1$$
$$H_n = \begin{bmatrix} H_{n-1} & H_{n-1} \\ H_{n-1} & -H_{n-1} \end{bmatrix} \tag{17}$$

where H_n is an $n \times n$ Hadamard matrix. This implies that the correlator of the CDMA demodulator can be implemented using fast Hadamard transform techniques.

III. CDMA System Model

In the multiple-access system for image transmission of interest, transmitters are assumed to share a radio band in a combination of the time and code domains. One way of multiple accessing in the code domain is spread spectrum, which is a signaling scheme that uses a much wider bandwidth than necessary for a given rate. Our model is based on a SS-CDMA system with binary phase shift keyed (BPSK) signaling, and a correlation receiver [16]. There are a total of K users transmitting over a common channel. Associated with each user $k \in 1, 2, \cdots, K$ is a data signal, $b_k(t)$ and a signature code waveform, $a_k(t)$ which are functions of time. They are defined by

$$b_k(t) = \sum_{i=-\infty}^{\infty} b_{k,i} \prod_{T}(t - iT) \tag{18}$$

$$a_k(t) = \sum_{j=-\infty}^{\infty} a_{k,j} \prod_{T_c}(t - jT_c) \tag{19}$$

where $b_{k,i} \in \{+1, -1\}$ denotes the kth user's information bit in the ith time interval, $a_{k,j}$ is an infinite random signature code sequence assigned to the kth user with each chip $a_{k,j}$ independent and equiprobably distributed on $+1$, -1, and $\prod_T(\cdot)$ is the unit pulse function of duration T, defined by

$$\prod_{T}(t) = \begin{cases} 1 & t \in [0, T) \\ 0 & \text{elsewhere} \end{cases}. \tag{20}$$

The duration of each data bit is T, while the duration of each chip in the signature code signal is T_c As a result, the number of chips per bit is $N_c = T/T_c$, where N_c is an integer and usually called the length of the spreading sequence.

Each user generates a signal $s_k(t)$ by modulating the data signal by its signature code signal and a carrier waveform, with the result

$$s_k(t) = \sqrt{2P_k}\, a_k(t) b_k(t) \cos(w_c t + \phi_k) \tag{21}$$

where P_k is the signal power, w_c is the carrier frequency, and ϕ_k is a random phase, uniformly distributed on the interval $(0, 2\pi)$.

A correlation receiver receives the signal $r(t)$ which is the sum of delayed versions of all transmitted signals and thermal noise. The received signal $r(t)$ is

$$r(t) = \sum_{k=1}^{K} s_k(t - \tau_k) + n(t) \tag{22}$$

where $n(t)$ is a white Gaussian channel noise with two-sided power spectral density $N_0/2$, and τ_k denotes the relative time delay between the kth user and base station. The synchronous correlation receiver recovers the transmitted data bit by correlating $r(t)$ with the kth signature PN code to construct decision statistics $Y_{k,i}$, where

$$Y_{k,i} = \int_{(i-1)T}^{iT} r(t) \cos[w_c(t - \tau_k) + \phi_k] a_k(t - \tau_k)\, dt. \tag{23}$$

The estimate $\hat{b}_{k,i}$ of the data bit $b_{k,i}$ is determined based on the rule

$$\hat{b}_{k,i} = \begin{cases} 1 & Y_{k,i} \geq 0 \\ -1 & Y_{k,i} \leq 0 \end{cases}. \tag{24}$$

A bit error occurs if $\hat{b}_{k,i} \neq b_{k,i}$.

In addition to the general system, symbol-synchronous CDMA systems will be also considered. Synchronous systems find applications in time slotted channels with a base station transmitting to remote mobile units and also in relays between control stations. The K users maintain time synchronism, therefore, in the model described above, the relative time delays associated with all users are assumed to be zero, i.e., $\tau_k = 0$. The synchronous problem will also be constructed for providing a manageable setting to better understand the issues in the more general and difficult asynchronous scenario. In this paper, we are particularly interested in applying the synchronous CDMA systems to the transmission of subband images.

IV. Image Quality Evaluation for Monochrome and Color Subband Image Transmission Over CDMA AWGN Channels

The SS-CDMA technique discussed in Section III can also be applied to the transmission of more than one image via the same limited radio band simultaneously. For N images transmitted at N different positions, each of them is divided into M subband images which have their corresponding signature codes. The transmitted signal $s_{kj}(t)$ of the kth subband of the jth image is expressed as

$$s_{kj}(t) = \sqrt{2P}\, a_k^{(j)}(t) b_k^{(j)}(t) \cos(w_c t + \phi_{kj}) \tag{25}$$

where $a_k^{(j)}(t)$ and $b_k^{(j)}(t)$ are a signature waveform and a data signal for the kth subband of the jth image, respectively, P is the signal power, ϕ_{kj} is a random phase and $1 \leq k \leq M$, $1 \leq j \leq N$.

Assume that these $M \times N$ subbands maintain the time synchronism in the SS-CDMA systems. Thus, the received

signal $r(t)$ is given by

$$r(t) = \sum_{j=1}^{N} \sum_{k=1}^{M} \sqrt{2P}\alpha_k^{(j)} a_k^{(j)}(t) b_k^{(j)}(t) \cdot \cos(w_c t + \phi_{kj}) + n(t) \quad (26)$$

where $\alpha_k^{(j)}$ is a channel amplitude distortion factor for the kth subband of the jth image. These channel amplitude distortion factors are affected by path loss and shadowing; e.g., a power loss phenomenon due to physical structure blocking the transmission path between a receiver and a transmitter. It should be mentioned that $\alpha_k^{(j)} = \alpha_1^{(j)} = \alpha^{(j)}$ for $1 \le k \le M$ and $1 \le j \le N$ since each subband in the same image is transmitted at the same position and then contributes the channel amplitude distortion factor of the same strength. At a SS-CDMA receiver, the received power from a nearer transmitter can be much bigger than that of a farther transmitter, causing interference and hence degrading the communication quality of the farther transmitter. This is called the near-far problem. Ideally, the received signals are intended to be received with equal power, but are actually different (random) when received. A number of power control mechanisms [17], [18] are trying to compensate for the differing received power and thus keeping the received powers (amplitudes) almost equal.

A. Intra- and Inter-Image Multi-Access Interferences

Suppose that a receiver consisting of M coherent BPSK SS-CDMA correlation demodulators is used to recover a specific image, where each correlation demodulator is trying to match its corresponding subband belonging to the image. The M recovered subbands are upsampled and reassembled by the synthesis filters into a close approximation to the image. For simplicity, we are interested in the correlation demodulator for the first subband of image 1. From (23), the output of the reference correlation receiver, $Y_{1,i}^{(1)}$, during the ith symbol interval for the reference subband and user is given by

$$Y_{1,i}^{(1)} = \int_{(i-1)T}^{iT} r(t) a_1^{(1)}(t) \cos(w_c t)\, dt. \quad (27)$$

The above integral can be broken up into the sum of four terms. We will assume that $w_c \gg T^{-1}$, and that, due to the post-detection, the double frequency terms occurring in $r(t)\cos(w_c t)$ can be neglected. The signal term is written as

$$Y_s = \int_{(i-1)T}^{iT} \sqrt{2P}\,\alpha_1^{(1)} [a_1^{(1)}(t)]^2 b_1^{(1)}(t) \cos^2(w_c t)\, dt = \sqrt{\frac{P}{2}}\,\alpha^{(1)} \int_{(i-1)T}^{iT} b_1^{(1)}(t)\, dt. \quad (28)$$

The variance of Y_s is found to be $[\alpha^{(1)} PT]$. The multiple-access interference term (MAI term) can be divided into two terms. The first MAI term, called the intra-image interference term, is generated from the inter-subbands in the same image, and can be expressed as

$$Y_{m,1} = \sqrt{\frac{P}{2}}\,\alpha^{(1)} \sum_{k=2}^{M} v_k \cos(\phi_{k1}) \quad (29)$$

where

$$v_k = \int_{(i-1)T}^{iT} a_k^{(1)}(t) a_1^{(1)}(t) b_k^{(1)}(t)\, dt. \quad (30)$$

The second MAI term, called the inter-image interference term, is generated from the subbands in the inter-images, and can be written as

$$Y_{m,2} = \sqrt{\frac{P}{2}} \sum_{j=2}^{N} \alpha^{(j)} \sum_{k=1}^{M} v_{k,j} \cos(\phi_{kj}) \quad (31)$$

where

$$v_{kj} = \int_{(i-1)T}^{T} a_k^{(j)}(t) a_1^{(1)}(t) b_k^{(j)}(t)\, dt. \quad (32)$$

The noise term is given by

$$Y_n = \int_{(i-1)T}^{iT} n(t) a_1^{(1)}(t) \cos(w_c t)\, dt. \quad (33)$$

The noise term is a white Gaussian noise having the variance of $N_0 T/4$.

The components of both intra-image and inter-image MAI terms are assumed to be pairwise independent and to contribute additional additive white Gaussian noises at the front of the reference correlation demodulator.

According to (32) in Pursley's report [16], it can be shown that the conditional variance of total interference and noise for the reference demodulator is given by

$$I = \text{var}\{Y_{1,i}^{(1)} | b_{1,i}^{(1)} = +1\} = \frac{N_0 T}{4} + \frac{PT^2}{2}\,\text{var}[\alpha^{(1)}] \cdot \left[\sum_{k=2}^{M} \sigma_k^2 + \sum_{j=2}^{N} \eta^{(j)} \left(\sum_{k=1}^{M} \sigma_{kj}^2\right)\right] \quad (34)$$

where $Y_{1,i}^{(1)}$ is the decision statistics for the reference demodulator defined in (27), $\eta^{(j)} = \{\text{var}[\alpha^{(j)}]/\text{var}[\alpha^{(1)}]\}$, $\text{var}[\alpha^{(j)}]$ denotes the variance of $\alpha^{(j)}$, and σ_k^2 and σ_{kj}^2 are the variances of v_i and v_{kj}, respectively. The conditional mean for the reference demodulator is

$$S = E\{Y_{1,i}^{(1)} | b_{1,i}^{(1)} = +1\} = \sqrt{\frac{P \cdot \text{var}[\alpha^{(1)}]}{2}}\, T. \quad (35)$$

As shown in Pursley's report [16], the signal-to-noise ratio for the reference demodulator is defined by

$$\text{SNR} = S \times I^{-(1/2)} = \left\{\frac{N_0}{2E_b} + \sum_{k=2}^{M} \sigma_k^2 + \sum_{j=2}^{N} \eta^{(j)} \left[\sum_{k=1}^{M} \sigma_{kj}^2\right]\right\}^{-(1/2)} \quad (36)$$

where E_b is the received energy per data bit ($E_b = PT \cdot \text{var}\{\alpha^{(1)}\}$). Note that Pursley's definition is slightly different from that of the other reports [17]–[19]. The term, E_b/N_0 is always called the channel signal-to-noise ratio.

Fig. 4. Test image "Portrait."

Fig. 5. test image "Andes."

Furthermore, Turin [19] showed that the variances of both v_k and v_{kj} are identical and can be written as, approximately,

$$\begin{aligned}\sigma_k^2 &= \text{var}\{v_k\} \\ &= \text{var}\{v_{kj}\} \\ &= \sigma_{kj}^2 \\ &\approx \frac{2T^2}{3N_c}\end{aligned} \tag{37}$$

where N_c is the length of the spreading sequence.

Substituting (37) into (36), (36) becomes

$$\text{SNR} = \left(\frac{N_0}{2E_b} + \frac{2T^2}{3N_c}\left\{M\left[\sum_{j=2}^{N}\eta^{(j)} + 1\right] - 1\right\}\right)^{(-1)/2}. \tag{38}$$

After applying a perfect power control to the SS-CDMA system, $\eta^{(j)}$ would become unity for $2 \le j \le N$. Thus, SNR would become

$$\text{SNR} = \left[\frac{N_0}{2E_b} + \frac{2T^2}{3N_c}(MN-1)\right]^{(-1)/2}. \tag{39}$$

Moreover, for the application of video telephone, the interference term can be reduced by a factor of 8/3 because the video activity factor of video telephone would be often identical to its associated voice activity factor (=3/8) during the video telephone conversations. Thus with both video and voice activity monitoring, the SNR is increased relative to (39) to become

$$\text{SNR} = \left[\frac{N_0}{2E_b} + \frac{T^2}{4N_c}(MN-1)\right]^{(-1)/2}. \tag{40}$$

For the transmission of color image over a CDMA AWGN channel, there are three signal-to-noise ratios for the reference demodulator defined by

$$\begin{aligned}\text{SNR}_Y = \Bigg[&\frac{N_0}{2E_b} + \left(\sum_{k=2}^{M_Y}\sigma_{Yk}^2 + \sum_{S=I,Q}\sum_{k=1}^{M_S}\sigma_{Sk}^2\right) \\ &+ \sum_{j=2}^{N}\eta^{(j)}\left(\sum_{S=Y,I,Q}\sum_{k=1}^{M_S}\sigma_{Skj}^2\right)\Bigg]^{-1/2}\end{aligned} \tag{41}$$

$$\begin{aligned}\text{SNR}_I = \Bigg[&\frac{N_0}{2E_b} + \left(\sum_{k=2}^{M_I}\sigma_{Ik}^2 + \sum_{S=Y,Q}\sum_{k=1}^{M_S}\sigma_{Sk}^2\right) \\ &+ \sum_{j=2}^{N}\eta^{(j)}\left(\sum_{S=Y,I,Q}\sum_{k=1}^{M_S}\sigma_{Skj}^2\right)\Bigg]^{-1/2}\end{aligned} \tag{42}$$

$$\begin{aligned}\text{SNR}_Q = \Bigg[&\frac{N_0}{2E_b} + \left(\sum_{k=2}^{M_Q}\sigma_{Qk}^2 + \sum_{S=Y,I}\sum_{k=1}^{M_S}\sigma_{Sk}^2\right) \\ &+ \sum_{j=2}^{N}\eta^{(j)}\left(\sum_{S=Y,I,Q}\sum_{k=1}^{M_S}\sigma_{Skj}^2\right)\Bigg]^{-1/2}\end{aligned} \tag{43}$$

where SNR_Y, SNR_I, and SNR_Q are the signal-to-noise ratios for Y-, I-, and Q-signals, respectively, and σ_{Yk}^2, σ_{Ik}^2, σ_{Qk}^2, σ_{Ykj}^2, σ_{Ikj}^2, and σ_{Qkj}^2 are their associated variances. Similarly, according to Turin's analysis, those variances are identical and have a value nearly equal to $(2T^2/3N_c)$. Thus, the expressions of (41)–(43) reduce to

$$\begin{aligned}\text{SNR}_Y &= \text{SNR}_I \\ &= \text{SNR}_Q \\ &\approx \left(\frac{N_0}{2E_b} + \frac{2T^2}{3N_c}\left\{(M_Y + M_I + M_Q)\right.\right. \\ &\quad \left.\left.\cdot\left[\sum_{j=2}^{N}\eta^{(j)} + 1\right] - 1\right\}\right)^{-1/2}.\end{aligned} \tag{44}$$

(a) (b)

(c) (d)

Fig. 6. (a) The lowest band x_{ll}. (b) The horizontal band x_{hl}. (c) The vertical band x_{lh}. (d) The diagonal band x_{hh}

After using a perfect power control and with monitoring the video activity, (44) becomes

$$\begin{aligned} \mathrm{SNR}_Y &= \mathrm{SNR}_I \\ &= \mathrm{SNR}_Q \\ &\approx \left\{ \frac{E_b}{2N_0} + \frac{T^2}{4N_c} \left[(M_Y + M_I + M_Q)N - 1 \right] \right\}^{-1/2}. \end{aligned} \tag{45}$$

B. Analysis of CDMA AWGN Channel Errors in Monochrome Subband Image Transmission

For the transmission of M subbands over the CDMA AWGN channel, Katto and Yasuda [23] showed that the reconstruction error variance of an image via these M parallel independent virtual channels can be obtained by a weighted sum of M subband reconstruction error variances:

$$\sigma^2_{image} = \sum_{k=1}^{M} \beta_k \sigma^2_{sk} \tag{46}$$

where β_k denotes the weighting value for the kth subband. More details of determining the values of β_k's can be found in [22]. From Cheong *et al.*'s results [22], it turns out that SSKF has low values compared to that of both QMF and orthonormal wavelets. In (46), σ^2_{sk} represents the error variance of the kth received subband in the reference image via a virtual connection over the AWGN channel created by its corresponding kth PN code. For subband image transmission via CDMA AWGN channels, there are two coding techniques for subband images. The baseband is encoded using DPCM, and higher bands are PCM encoded. In other words, σ^2_{s1} can be denoted by $\sigma^2_{r,\mathrm{DPCM}}$ which is the reconstruction error variance for the DPCM coding of subband. σ^2_{sk}, $k \geq 2$ are used to characterize the reconstruction error variances for PCM-encoded high frequency bands and can be denoted by $\sigma^2_{r,\mathrm{PCM}}$'s.

Jayant and Noll [21] showed that $\sigma^2_{r,\mathrm{PCM}}$ are expressed as

$$\begin{aligned} \sigma^2_{r,\mathrm{PCM}} &\approx \sigma^2_{q,\mathrm{PCM}} + \sigma^2_c \\ &\approx (\epsilon^2_{q,\mathrm{PCM}} + \epsilon^2_c)\sigma^2_x \end{aligned} \tag{47}$$

where $\sigma^2_{q,\mathrm{PCM}}$, $\epsilon^2_{q,\mathrm{PCM}}$, σ^2_c, and ϵ^2_c are the quantization error variance, PCM quantizer performance factor, channel error

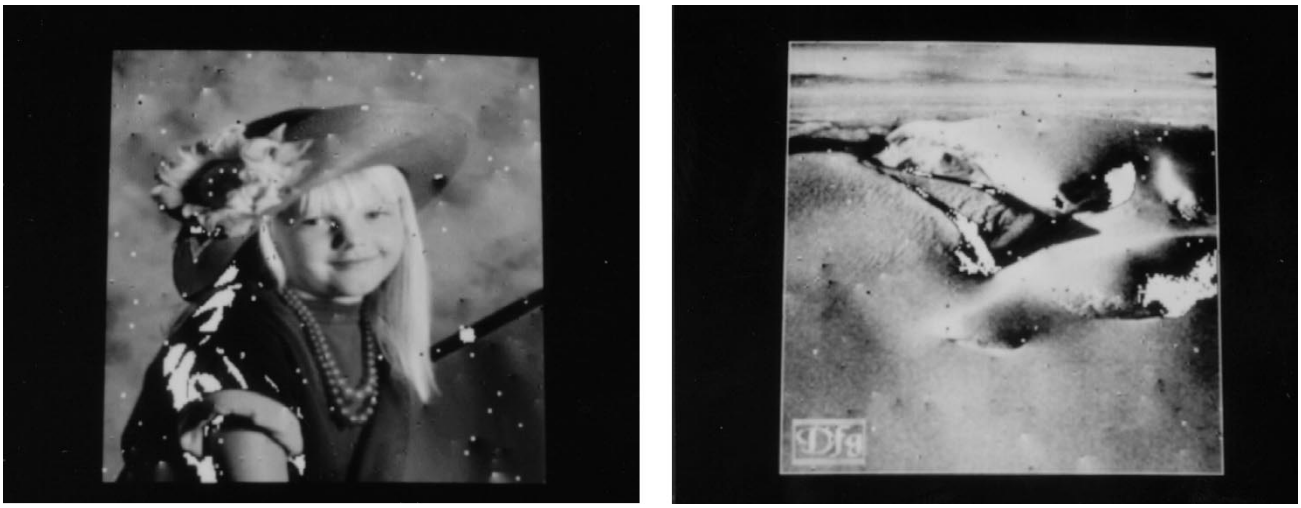

(a) (b)

Fig. 7. (a) The reconstructed "Portrait" image via perfect power controlled SS-CDMA AWGN channels without RM-1 channel coding when $E_b/N_0 = 6$ dB. (b) The reconstructed "Andes" image via perfect power controlled SS-CDMA AWGN channels without RM-1 channel coding when $E_b/N_0 = 6$ dB.

(a) (b)

Fig. 8. (a) The reconstructed "Portrait" image via perfect power controlled SS-CDMA AWGN channels with RM-1 channel coding when $E_b/N_0 = 6$ dB. (b) The reconstructed "Andes" image via perfect power controlled SS-CDMA AWGN channels with RM-1 channel coding when $E_b/N_0 = 6$ dB.

variance, and PCM channel performance factor, respectively. Note that the crosscorrelation between quantization and channel error is nearly equal to zero if the quantizer characteristics is close to that of an optimal quantizer. Moreover, Noll [20] found that the channel performance factor ϵ_c^2 can be expressed in terms of bit error probability, p_e, and is given by

$$\epsilon_c^2 = \sum_{j=1}^{R} \xi_j p_e^j \tag{48}$$

where R is the number of bits used to represent the quantizer output and ξ_j's are channel coefficients that reflect the effects on σ_c^2 of the quantizer characteristics, the chosen binary code and the source statistics. For example, $\xi_1 = 2.55$, $\xi_2 = 4.97$, $\xi_3 = 6.91$ when natural binary code is chosen and a nonuniform quantizer is used. Pursley [16] showed that the bit error probability for CDMA channel with an additive white Gaussian noise is

$$p_e = \begin{cases} Q(\text{SNR}) \\ \quad \text{without RM channel coding} \\ \dfrac{2^{n-1}}{2^n - 1}\left[1 - \displaystyle\int_{-\infty}^{\infty} \frac{\exp(-x^2)}{\sqrt{\pi}} \right. \\ \quad \left. \cdot Q(-x - \sqrt{n}\text{SNR})^{2^n - 1}\, dx\right] \\ \quad \text{with } (2^n, n) \text{ RM channel coding} \end{cases} \tag{49}$$

where $Q(\cdot)$ is the standard Gaussian integral function. Note that $p_e = Q(\sqrt{\text{SNR}})$ when the expression of SNR is characterized by the definition of [17]–[19] and the SS-CDMA systems do not involve the RM channel coding.

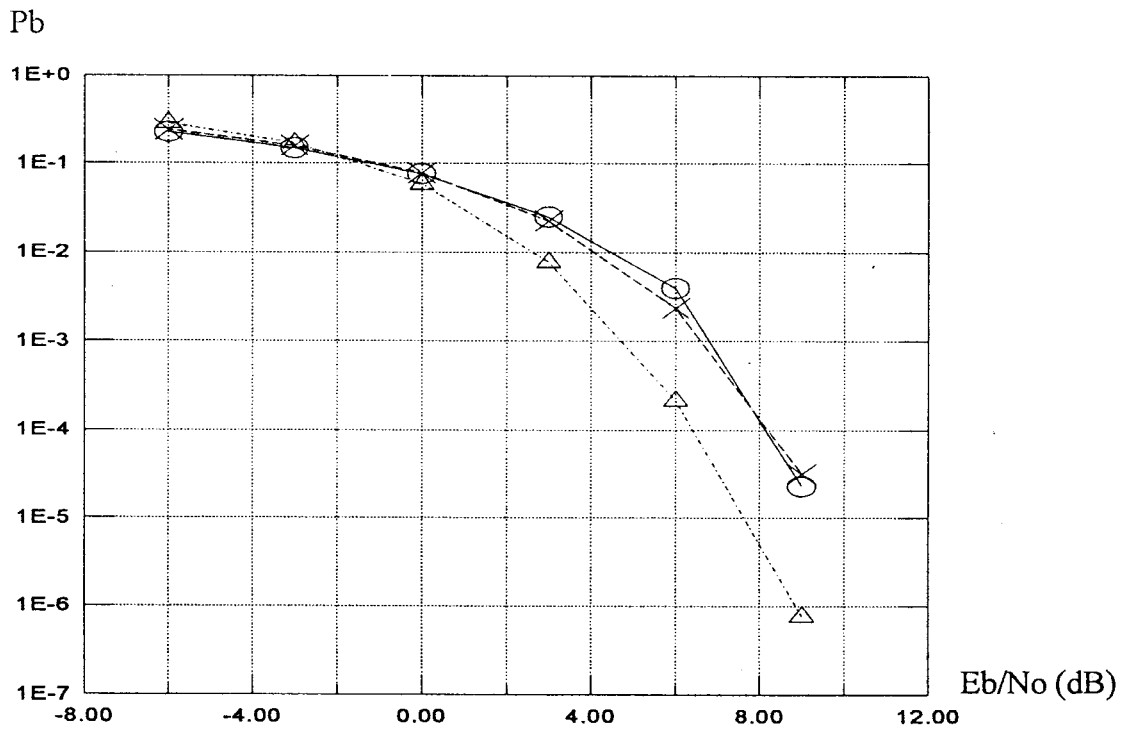

Fig. 9. The bit error rate of the "Portrait" image via perfect power controlled SS-CDMA AWGN channels. (×: theoretic bit error rate, ○: bit error rate without RM-1 coding, △: bit error rate with RM-1 coding.

Additionally, Jayant and Noll [21] also showed that the reconstruction error variance for DPCM can be approximately expressed as the sum of both the quantization error variance and the channel error variance since the crosscorrelation has been found to be negligible compared to these two factors. Moreover, they showed that the DPCM channel performance factor $\epsilon^2_{c,\,\mathrm{DPCM}}$ can be approximately expressed as: $\epsilon^2_{c,\,\mathrm{DPCM}} \approx \gamma\epsilon^2_{c,\,\mathrm{PCM}} = \gamma\epsilon^2_c$, where γ is called the power transfer factor of the decoder filter of the DPCM. Thus, it yields

$$\begin{aligned}\sigma^2_{r,\,\mathrm{DPCM}} &\approx \sigma^2_{q,\,\mathrm{DPCM}} + \sigma^2_{c,\,\mathrm{DPCM}} \\ &\approx (\epsilon^2_{q,\,\mathrm{DPCM}} + \epsilon^2_{c,\,\mathrm{DPCM}})\sigma^2_\epsilon \\ &\approx (\epsilon^2_{q,\,\mathrm{DPCM}} + \gamma\epsilon^2_c)\sigma^2_x G_p^{-1} \end{aligned} \tag{50}$$

where $\epsilon^2_{q,\,\mathrm{DPCM}}$ is the DPCM quantizer performance factor, σ^2_ϵ is the prediction error variance, and G_p is the prediction gain which is defined as the ratio between the input signal variance and the prediction error variance.

Substituting (47) and (50) into (46), we have

$$\begin{aligned}\sigma^2_{image} = &\left(\sum_{k=1}^{M} \beta_k \epsilon^2_{qk}\right)\sigma^2_x \\ &+ \left(\beta_1\gamma\epsilon^2_{c1}G_p^{-1} + \sum_{k=2}^{M}\beta_k\epsilon^2_{ck}\right)\sigma^2_x \end{aligned} \tag{51}$$

where ϵ^2_{q1} is the DPCM quantizer performance factor, ϵ^2_{qk}, $k \geq 2$ denote the PCM quantizer performance factors, and ϵ^2_{ck}'s are the channel performance factors. In (51), the first and second terms represent the total quantization error variance and the total channel error variance, respectively. Recently, Irie and Kishimoto [9] and Lu, Omar, and Zhang [24] proposed an modified symmetric short-kernel filters discussed in Section II which can achieve quantization-error-free reconstruction for the subband images when more than 10 b, $R \geq 10$, are used to represent the quantization levels of PCM and DPCM codings for the subbands. As a result, the first term of (51) vanishes. Thus, the expression of (51) reduces to

$$\sigma^2_{image} \approx \left(\beta_1\gamma\epsilon^2_{c1}G_p^{-1} + \sum_{k=2}^{M}\beta_k\epsilon^2_{ck}\right)\sigma^2_x. \tag{52}$$

From (2), the peak signal-to-noise ratio (PSNR) of the reconstructed image can be expressed as a form in terms of channel performance factors according to the similar procedure proposed by our companion papers [28] and [29]:

$$\begin{aligned}\mathrm{PSNR} \approx &10\log_{10}\left(\frac{x^2_{pp}}{\sigma^2_x}\right) \\ &- 10\log_{10}\left(\beta_1\gamma\epsilon^2_{c1}G_p^{-1} + \sum_{k=2}^{M}\beta_k\epsilon^2_{ck}\right). \end{aligned} \tag{53}$$

Moreover, the channel contributes ϵ^2_{ck}'s only through single errors when p_e and R are sufficiently small. Therefore, $\epsilon^2_{ck} \approx \xi_1^k p_e$ for the kth subband, and PSNR of (53) becomes as follows:

$$\mathrm{PSNR} \approx C - 10\log_{10} p_e \tag{54}$$

where $C = 10\log_{10}(x^2_{pp}/\sigma^2_x) - 10\log_{10}(\beta_1\gamma\xi_1^1 G_p^1 + \sum_{k=2}^{M}\beta_k\xi_1^k)$ is a constant which is independent of the bit error rate. From (54), PSNR is inversely related to a simple logarithmic function of p_e when p_e becomes sufficiently small.

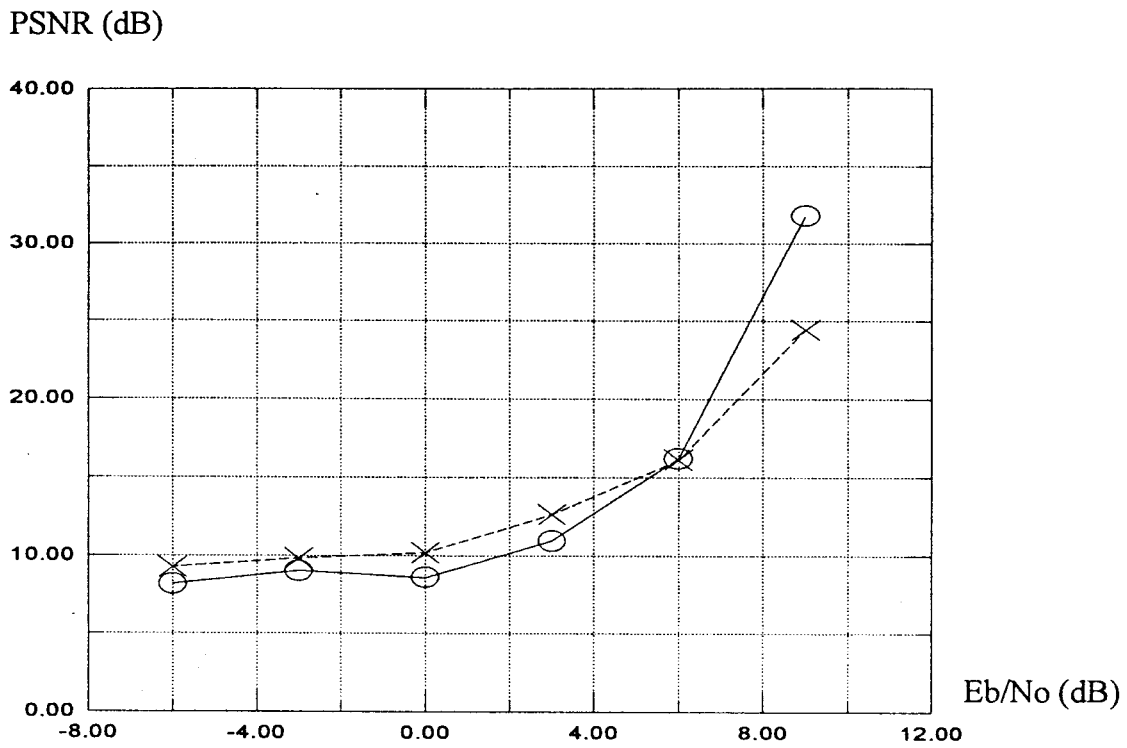

Fig. 10. PSNR performance versus channel SNR for "Portrait" and "Andes" images via SS-CDMA AWGN channels without RM-1 channel coding (◯: Portrait image, ×: Andes image).

In practice, σ_r^2 for an $m \times m$ monochrome image can be obtained by computing the empirical mean square error given by

$$\sigma_r^2 = \left(\frac{1}{m}\right)^2 \sum_{i=1}^{m} \sum_{j=1}^{m} (x_{ij} - y_{ij})^2 \tag{55}$$

where x_{ij} and y_{ij} represent the gray values of the (i, j) pixel of both input and output images, respectively.

C. Analysis of CDMA AWGN Channel Errors in Color Subband ImageTransmission

Westerink *et al.* [13] have proposed a color distortion measure that is additive with respect to the individual color component mean-squared errors in the YIQ domain. The expression of the YIQ color distortion measure for the reconstructed color picture via SS-CDMA AWGN channels is given by

$$D_{\mathrm{YIQ}} = \omega_Y \sigma_{r,Y}^2 + \omega_I \sigma_{r,I}^2 + \omega_Q \sigma_{r,Q}^2 \tag{56}$$

where $\sigma_{r,Y}^2$, $\sigma_{r,I}^2$, and $\sigma_{r,Q}^2$ are the reconstruction error variances for Y-, I-, and Q-signals, respectively, and ω_Y, ω_I, and ω_Q are their corresponding positive weighting coefficients. For compatibility with distortion measures for monochrome images, ω_Y is equal to 1. However, experiments show that choosing lower values for ω_I and ω_Q than 1 yields better subjective results [13]. For example, $\omega_I = \omega_Q \approx 0.3$. By the similar procedure of deriving the reconstruction error variance for monochrome images, (56) becomes

$$D_{\mathrm{YIQ}} \approx \sum_{S=Y,I,Q} \omega_S \left(\beta_1^S \gamma \epsilon_{Sc1}^2 G_p^{-1} + \sum_{k=2}^{M_S} \beta_k^S \epsilon_{Sck}^2 \right). \tag{57}$$

From (44), it can be shown that the bit error probabilities for Y-, I-, and Q-signals are identical. In other words, $p_e^Y = p_e^I = p_e^Q = p_e$. Hence, their channel performance factor ϵ_{Sck}^2 can be expressed as follows:

$$\epsilon_{Sck}^2 = \sum_{j=1}^{R_S} \xi_j^{k,S} p_e^j \quad 1 \le k \le M_S,\ S = Y, I, Q. \tag{58}$$

From (57) and (58), when p_e is sufficiently small, D_{YIQ} of (56) becomes

$$D_{\mathrm{YIQ}} \approx C p_e \tag{59}$$

where C is a constant which is independent of the channel errors and given by

$$C = \sum_{S=Y,I,Q} \omega_S \left(\beta_1^S \gamma \xi_1^{1,S} G_p^{-1} + \sum_{k=2}^{M_S} \beta_k^S \xi_1^{k,S} \right). \tag{60}$$

From (59), it turns out that D_{YIQ} is proportional to the bit error rate, p_e when p_e is sufficiently small.

V. Simulation Results

Simulation results have been carried out to study the transmission of both the monochrome and color images over SS-CDMA AWGN channels. First, we are interested in investigating various aspects of the monochrome subband image

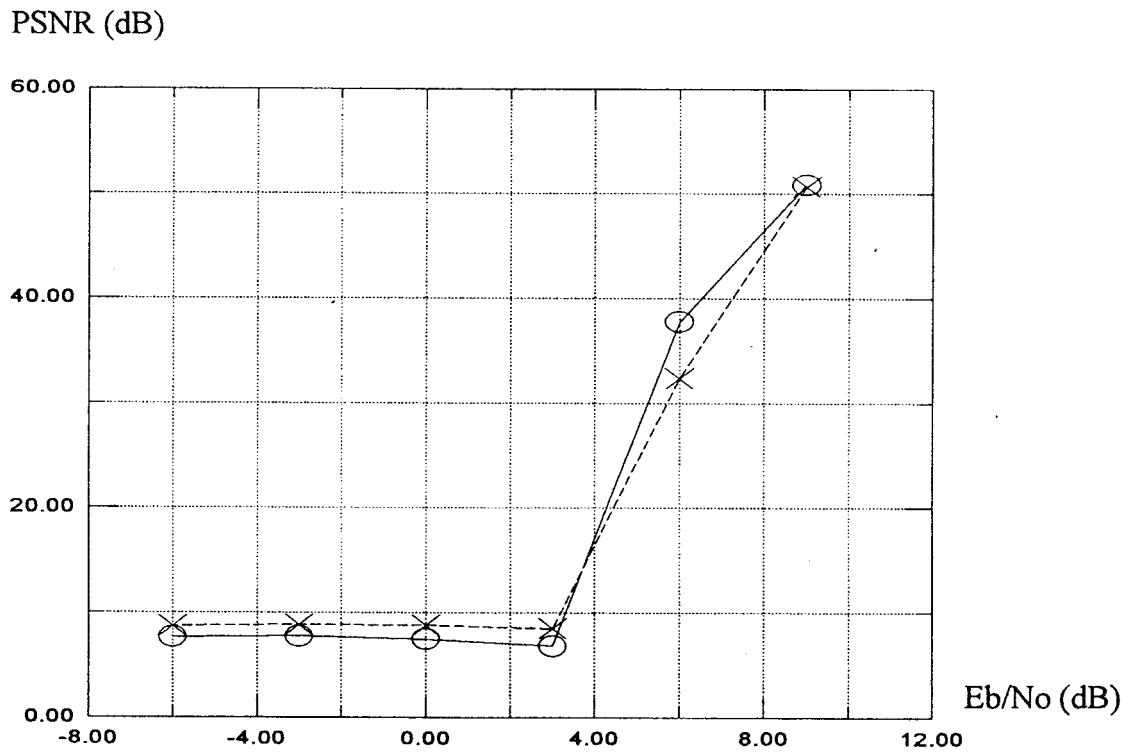

Fig. 11. PSNR performance versus channel SNR for "Portrait" and "Andes" images via SS-CDMA AWGN channels with RM-1 channel coding (○: Portrait image, ×: Andes image).

transmission. Specially, comparisons were made in terms of image quality, bit error rate, channel errors, and CDMA power control. The peak signal-to-noise ratio (PSNR) was used as the criteria for measuring monochrome image quality at the decoder output. In the remainder of this section, the YIQ color distortion measure performance evaluation of color subband image transmission via SS-CDMA AWGN channels is presented. In order analyze the performance of the transmission of monochrome subband images via SS-CDMA channels, two monochrome test images, "Portrait" illustrated in Fig. 4 and "Andes" illustrated in Fig. 5 are considered in our system. They are gray scale pictures with 256 × 256 pixels and 8 b per pixel. For each picture, the input was first split into four bands, shown in Fig. 6, using a modified two-dimensional separable SSKF (2-tap in each direction) proposed by Irie *et al*. [9] and [25]. The lowest band image was DPCM encoded using two-dimensional prediction and a nonuniform quantizer with ten quantization bits and subsequent variable length coding. However, since the samples in the higher frequency bands show little correlation among pixels, these bands are encoded using PCM with the 9-b nonuniform quantizer instead of DPCM. More recently, Irie *et al*. [9] and [25] and Lu *et al*. [24] showed that this nine-bit nonuniform quantizer for PCM coding is able to achieve an acceptably small quantization error as well as a 10-b quantizer.

Next, we consider the transmission of these two test pictures in a synchronous eight-user CDMA channel. Pseudo noise codes of our SS-CDMA system are generated by a four-shift register [18] and would be assigned to their corresponding subbands of both test images. The length of the spreading sequence, N_c, is found to be 15 $(=2^4-1)$. Assume that a perfect power control is applied to the SS-CDMA system and then keep the received powers of these eight subbands equal. This implies that $\eta^{(j)}$'s are equal to unity for $2 \leq j \leq 8$.

Moreover, the SS-CDMA channel output is corrupted by a zero-mean additive white Gaussian noise (AWGN). The channel signal-to-noise ratio of each subband is assumed to be 6 dB. Fig. 7 shows the reconstructed pictures of both Portrait and Andes without RM channel coding, and Fig. 8 shows the reconstructed pictures with RM channel coding where μ and m of RM code are chosen to be 1 and 3, respectively. Undoubtedly, the quality of the coded pictures shown in Fig. 8 is better than the uncoded pictures shown in Fig. 7 because the RM code removes the AWGN noise in the pictures of Fig. 7. The bit error probabilities were determined by simulating the CDMA subband image transmission and taking an average of 5.24 × 10^5 ($\approx$ 8 \times 256 × 256) bits in an image. In Fig. 9, the average bit-error probabilities of Portrait image without and with RM channel coding are plotted versus the channel signal-to-noise ratio, E_b/N_0, of its first subband. It is clear from this figure that the average bit-error probability without performing RM code is close to its theoretic bit-error probability of $p_e = Q[\mathrm{SNR}\,(E_b/N_0)] = f(E_b/N_0)$, where SNR defined in (39) can be expressed as a function of E_b/N_0. The average bit-error rate performance with RM coding is much better than the other two bit-error rate performances. The value of image PSNR is calculated by the equation: $\mathrm{PSNR} = 10\log_{10}(255^2/\sigma_r^2)$, where σ_r^2 is defined in (55). Fig. 10 illustrates the image PSNR versus channel SNR performances, E_b/N_0's, of both Portrait and Andes via SS-CDMA channel. These two PSNR curves are almost identical since the received powers of all the subbands are identical. In

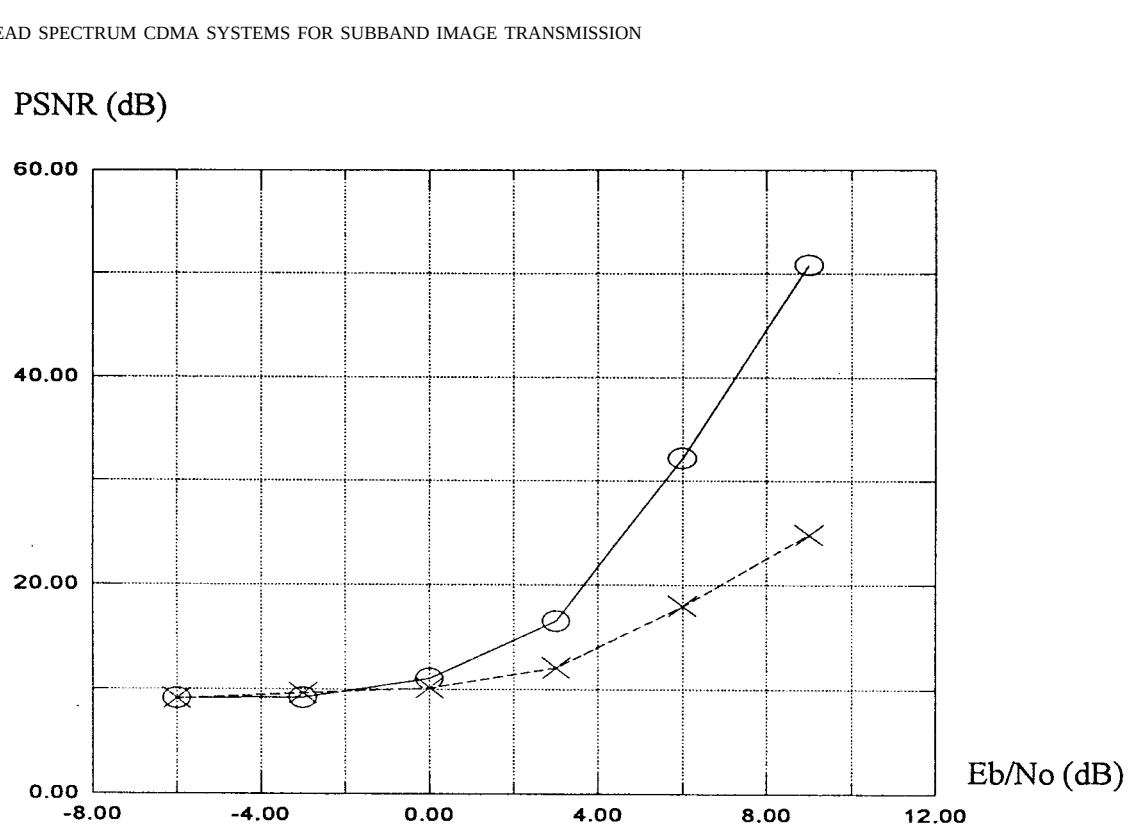

Fig. 12. PSNR performance versus channel SNR for "Portrait" and "Andes" images via SS-CDMA AWGN channels with RM-1 channel coding and with unequal received power difference, $P_2/P_1 = -6$ dB. (◯: Portrait image, ×: Andes image).

Fig. 10, the PSNR curve for Portrait is inversely related to the curve of bit-error rate shown in Fig. 9. This would verify the relationship of (54) when p_e is sufficiently small. However, PSNR is a complicated monotonically decreasing function of p_e when channel signal-to-noise ratio value falls within the interval between 2–6 dB. Fig. 11 shows the PSNR values for both Portrait and Andes with RM channel coding which are much greater than the PSNR values without RM channel coding since the bit-error rate values of coded CDMA systems are smaller than that of uncoded systems. The quality of image transmission via coded CDMA systems rapidly breaks down with the image PSNR becoming an unreliable quality measure when the channel SNR value is lower than 3 dB. It may be observed from Figs. 10 and 11 that the coded systems attain almost the same 4-dB channel SNR improvement at an image PSNR of 30 dB relative to the uncoded systems. The PSNR of 30 dB is a practical performance index which allows error-free image transmission [21].

The SS-CDMA systems would suffer from a severe near-far problem when the received powers of the system are not perfectly controlled. Fig. 12 compares the respective PSNR's for Portrait and Andes achieved by uncoded SS-CDMA systems where $\eta^{(2)} = P_2/P_1 = \text{var}\{\alpha^{(2)}\}/\text{var}\{\alpha^{(1)}\} = \frac{1}{2}$ or -6 dB, where P_1 and P_2 denote the received powers for Portrait and Andes, respectively. As expected, the quality of the received image (Portrait) from a nearer position is much better than that of the received image (Andes) from a farther position. Comparing Fig. 12 with Fig. 10, the PSNR of Portrait of Fig. 12 is larger than that of Fig. 10 since Andes of Fig. 12 produces smaller interference strength to Portrait than Andes of Fig. 10. However, the PSNR of Andes of Fig. 12 is smaller than that of Fig. 10 since it is corrupted by a large interference caused from Portrait of Fig. 12. Similarly, Fig. 13 shows the coded systems can improve the quality of both received pictures via the uncoded systems. It should be mentioned that the coded system allows the error-free image transmission from the nearer position at a channel SNR value larger than 2 dB. However, the error-free image transmission via coded systems from the farther position is achieved at a channel SNR value larger than 7 dB. This performance degradation ($\approx$5 dB) is resulted from the unequal received power difference, $P_2/P_1 = -6$ dB.

In order to investigate the performance of the multi-code CDMA system with PN codes for color image transmission, we test the system using two color images with their corresponding file names, i.e., frames.jpg and window.jpg in the well-known image system called Adobe Photoshop. Frames.jpg and window.jpg are the 24-b RGB images of 677 $\times$ 576 pixels and 278 $\times$ 414 pixels, respectively. We use the image size command of Adobe Photoshop to resize both the color images into the desired test color pictures of the same image resolution, 256 $\times$ 256 pixels. Next, a RGB/YIQ transform of (1) is conducted to transfer each RGB color image to its associated YIQ components. For simplicity, it is assumed that each component is then decomposed into four subbands. As a result, $M_Y = M_I = M_Q = 4$. Thus, the transmission of the these two test color images is the same as a transmission of 24 users over a CDMA AWGN channel, where a PN code of length 127 is assigned to each subband. Furthermore, it is assumed that both a perfect power control and a first order RM code of length 7 are applied to our system. Fig. 14 illustrates the YIQ color distortion measure versus channel SNR of both

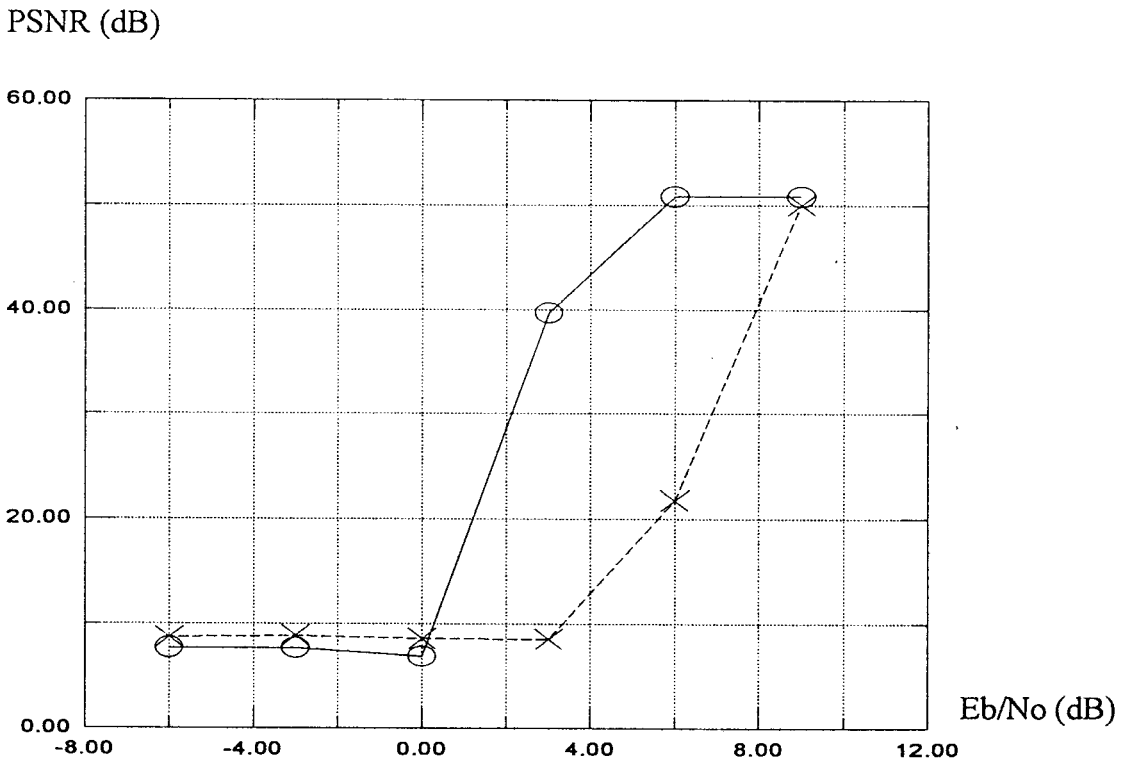

Fig. 13. PSNR performance versus channel SNR for "Portrait" and "Andes" images via SS-CDMA AWGN channels with RM-1 channel coding and with unequal received power difference, $P_2/P_1 = -6$ dB. (◯: Portrait image, ×: Andes image).

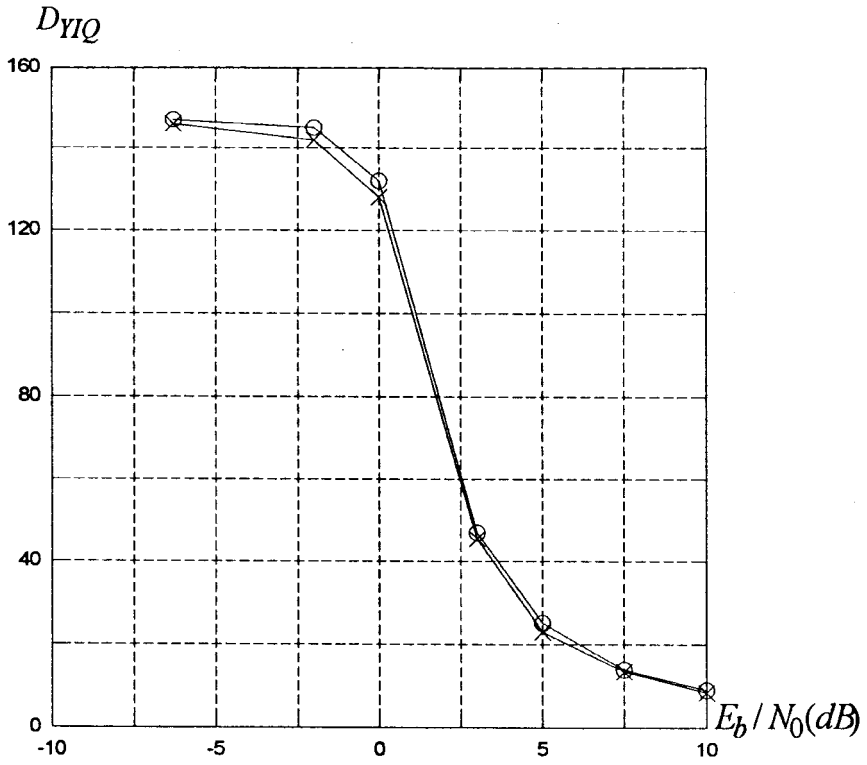

Fig. 14. YIQ color distortion measure versus channel SNR for "Window" and "Frames" color images via perfect power controlled SS-CDMA AWGN channels with RM-1 channel coding (◯: Window image and ×: Frames image).

color images via SS-CDMA AWGN channel. It is clear from this figure that the YIQ color distortion measure is a decreasing function of E_b/N_0 which will fall within the perceptual color vision criteria ($\approx$16) [13] when the value of E_b/N_0 is greater than 6 dB. Finally, it may reduce the total number of PN codes for chrominance signals since Gharavi *et al.* [7] have shown

that the reconstructed color image quality is still maintained when the higher bands for I and Q signals are discarded.

VI. Conclusion

In this paper, we have proposed a new scheme of image transmission system over SS-CDMA AWGN channels. A subband coding process is proposed to divide the image information into a number of data streams, each of which is transmitted using one of signature PN codes, and then spread to full channel bandwidth. The multi-code CDMA system allows these multiple data streams to be transmitted and be accessed simultaneously over the same limited channel bandwidth. A modified short-kernel filters have been proposed for achieving the quantization-error-free reconstruction at a very low bit rate for the subband image transmission via the SS-CDMA AWGN channels. Thus, the total reconstruction error depends on a quantity due solely to channel errors. Additionally, we introduced an analysis of transmission error effects in both the monochrome and color subband images via the SS-CDMA AWGN channels. Finally, several numerical examples and simulation results are conducted to demonstrate the usefulness of the proposed approach.

Acknowledgment

The author wishes to thank the reviewers for their valuable comments, which led to the improvements in this paper. Thanks also go to Dr. B. C. Wang and C. C. Chang for their programming efforts.

References

[1] CCITT Recommendation H.261, "Video codec for audiovisual services at $p \times 64$ kbit/s," Dec. 1990.
[2] N. MacDonald, "Transmission of compressed video over radio links," *Br. Telecom Technol. J.*, vol. 11, no. 2, Apr. 1993.
[3] W. C. Y. Lee, "Overview of cellular CDMA," *IEEE Trans. Veh. Technol.*, vol. 40, pp. 291–302, May 1991.
[4] R. M. Gagliardi, A. J. Mendez, M. R. Dale, and E. Park, "Fiber-optic digital video multiplexing using optical CDMA," *J. Lightwave Technol.*, vol. 11, no. 1, pp. 20–26, Jan 1993.
[5] K. I. Kitayama, "Novel spatial spread spectrum based fiber optic CDMA networks for image transmission," *IEEE J. Select. Areas Commun.*, vol. 12, pp. 762–772, May 1994.
[6] J. W. Woods and S. D. O'Neil, "Subband coding of images," *IEEE Trans. Acoust., Speech, Signal Processing*, vol. ASSP-34, pp. 1278–1288, Oct. 1986.
[7] H. Gharavi and A. Tabatabai, "Subband coding of monochrome and color images," *IEEE Trans. Circuits Syst.*, vol. 35, pp. 207–214, Feb. 1988.
[8] D. Le Gall and A. Tabatabai, "Subband coding of digital images using symmetric short kernel filters and arithmetic coding technique," in *IEEE Proc. ICASSP*, New York, Apr. 1988, pp. 761–764.
[9] K. Irie and R. Kishimoto, "A study on perfect reconstruction subband coding," *IEEE Trans. Circuits Syst. Video Technol.*, vol. 1, pp. 42–48, Mar. 1991.
[10] G. Karlsson and M. Vetterli, "Three dimensional subband coding of video," in *IEEE Proc. ICASSP*, Apr. 1988, pp. 1100–1103.
[11] M. Vetterli, "Multi-dimensional subband coding: Some theory and algorithms," *Signal Process.*, vol. 6, pp. 97–112, Apr. 1984.
[12] H. Gharavi and A. Tabatabai, "Subband coding of digital images using two-dimensional quadrature mirror filtering," in *Proc. SPIE Vis. Comm. Image Process.*, Cambridge, MA, Sept. 1986, vol. 707, pp. 51–61.
[13] P. H. Westerink *et al.*, "Subband coding of color images," in *Subband Image Coding*, J. W. Woods, Ed. MA: Kluwer Academic, 1991.
[14] H. Gharavi, "Subband coding of video signals," in *Subband Image Coding*, J. W. Woods, Ed. Boston, MA: Kluwer, 1991.
[15] S. Lin and Costello, *Error-Correcting Codes.* Englewood Cliffs, NJ: Prentice-Hall Inc., 1983.
[16] M. B. Pursley, "Spread spectrum multiple access communications," in *Multi-User Communication Systems.* New York: Springer-Verlag, 1981, pp. 139–199.
[17] K. S. Gilhousen *et al.*, "On the capacity of a cellular CDMA system," *IEEE Trans. Veh. Technol.*, vol. 40, no. 5, pp. 303–312, 1991.
[18] W. C. Y. Lee, "Power control in CDMA," in *Proc. Vehicular Technology Conf.*, 1991, pp. 77–80.
[19] G. L. Turin, "The effects of multipath and fading on the performance of direct-sequence CDMA systems," *IEEE J. Select. Areas Commun.*, vol. SAC-2, pp. 597–603, July 1984.
[20] P. Noll, "Effects of channel errors on the signal-to-noise performance of speech-encoding systems," *Bell Syst. Tech. J.*, pp. 1615–1636, Nov. 1975.
[21] N. S. Jayant and P. Noll, *Digital Coding of Waveforms.* Englewood Cliffs, NJ: Prentice-Hall, 1984.
[22] C. K. Cheong, K. Aizawa, T. Saito, and M. Hatori, "Subband image coding with biorthogonal wavelets," *IEEE Trans. Fundamentals*, vol. E75-A, pp. 871–880, July 1992.
[23] J. Katto and Y. Yasuda, "Performance evaluation of subband coding and optimization of its filter coefficients," in *Proc. SPIE Visual Comm. Image Proc.*, Boston, MA, Nov. 1991, pp. 95–106.
[24] C. C. Lu, N. Omar, and Y. Q. Zhang, " A modified short-kernel filter pair for perfect reconstruction of HDTV signals," *IEEE Trans. Circuits Syst. Video Technol.*, vol. 3, pp. 162–164, Apr. 1993.
[25] K. Irie, Y. Okumura, N. Sakurai, and R. Kishimoto, "High-quality subband codec for HDTV transmission," *IEEE Trans. Circuits Syst. Video Technol.*, vol. 4, pp. 195–200, Apr. 1994.
[26] R. Wyrwas, M. J. Miller, R. Anjaria, and W. Zhang, "Multimedia access options for multi-media wireless system," in *Proc. 3rd Workshop Third Generation Wireless Information Networks*, Rutgers University, Apr. 1992, pp. 289–294.
[27] C. L. I. and R. D. Gitlin, "Multi-code CDMA wireless personal communication networks," in *1995 IEEE 45th Vehicular Technology Conf.*, Chicago, IL, July 25–28, 1995, pp. 1060–1063.
[28] P. R. Chang and C. C. Chang, "Fiber-optic subcarrier multiplexed CDMA local area networks for subband image transmission," *IEEE J. Select. Areas Commun.*, vol. 14, no. 9, pp. 1866–1878, Dec. 1996.
[29] B. C. Wang and P. R. Chang, "Spread-spectrum multiple-access with DPSK modulation and diversity for image transmission over indoor radio multipath fading channels," *IEEE Trans. Circuits Syst. Video Technol.*, vol. 6, no. 2, pp. 200–214, 1996.

Po-Rong Chang (M'87) received the B.S. degree in electrical engineering from the National Tsing-Hua University, Taiwan, R.O.C., in 1980, the M.S. degree in telecommunication engineering from the National Chiao-Tung University, Hsinchu, Taiwan, in 1982, and the Ph.D. degree in electrical engineering from Purdue University, West Lafayette, IN, in 1988.

From 1982 to 1984, he was a Lecturer in the Chinese Air Force Telecommunication and Electronics School for his two-year military service. From 1984 to 1985, he was an Instructor of electrical engineering at National Taiwan Institute of Technology, Taipei. From 1989 to 1990, he was a Project Leader in charge of SPARC chip design team at ERSO of Industrial Technology and Research Institute, Chu-Tung, Taiwan. Currently, he is a Professor of Communication Engineering, National Chiao-Tung University. His current interests include wireless multimedia systems, CDMA systems, virtual reality, and fuzzy neural network.